**Adv. Studies Theor. Phys., Vol. 1, 2007, no. 7, 301 - 342**

# Smart Vibroacoustic Systems and Structures through Piezoelectric Actuators

**M. N. Ichchou**

LTDS UMR CNRS 5513, Equipe Dynamique des Systemes et des Structures
Ecole Centrale de Lyon
36 avenue Guy de Collongue
69134 Ecully, France

**B. Troclet**

EADS ST, 66, Route de Verneuil
BP 3002
78133 Les Mureaux Cedex, France

**Abstract**

The performances of any passive system can be improved by addition of an active technology. Such a technology can cure deficiencies of the passive system, and thus increases its operating range. Currently, such techniques start to emerge in the industrial world and give place to more and more applications and innovations. However, several problems arise during the synthesis of an active technology. These problems are mainly dependent on the nature of the phenomena to be treated and the frequency range of work. They condition thus, the control algorithms to be used and especially the technology of actuation. Concerning that last question, smart materials are the most commonly agreed answer. The offered overview here deals with some aspects of intelligent materials and structures when active insulation/filtration/absorption of undesirable vibrations and noise are in concern. Several smart materials suited for that purpose are reviewed. Among them, piezoelectric materials, ER/MR fluids and Shape Memory Alloys (SMA) are often considered. Here the focus is on piezoelectric abilities in smart systems and structures applications. To that purpuse, piezoelectric materials electromechanical representation is first offered. Some of their possible integration into smart structures proposed.

**Keywords:** Smart vibroacoustic systems, Piezoelectric actuators, Noise control

# 1 Piezoelectricity

Piezoelectricity is a coupling between a material's mechanical and electrical behaviors. In the simplest of terms, when a piezoelectric material is squeezed, an electric charge collects on its surface. Conversely, when a piezoelectric material is subjected to a voltage drop, it mechanically deforms. These effects can be sufficiently strong for some materials so that they can be, and in fact, they are widely used as sensors and actuators. We use two piezoelectric patches as an actuator in our model of active elasto-poroelastic sandwich panel.

In this section we shall briefly present the equations of linear piezoelectricity emphasizing the multiphysical character of this problem. Since the piezoelectricity is in fact a coupling effect completely realized in the constitutive relations only, the separate Section is devoted to these equations; in this Section we present different (though perfectly equivalent) forms of piezoelectric constitutive equations.

## 1.1 Equations of linear piezoelectricity

The piezoelectricity problem links two classical problems: the problem of continuum mechanics and the electrostatics' problem. The piezoelectric effect just couple both problems. Therefore, the following quantities (specific for each of the problems) are used:

$u_i$ – the mechanical displacements,
$\varphi$ – the electric field potential,
$S_{ij}$ – the strain tensor,
$E_i$ – the electric field vector,
$T_{ij}$ – the stress tensor,
$D_i$ – the electric displacement vector,
$f_i$ – the mechanical body forces,
$q$ – the electric body charge,
$\varrho$ – the mass density,
$c_{ijkl}$ – the elastic material constants,
$e_{kij}$ – the piezoelectric material constants,
$\epsilon_{ij}$ – the dielectric material constants.

Here, the only additional quantity which refers to the piezoelectric effect is the third-order tensor, $e_{kij}$, with components being the material piezoelectric properties.

The state of equilibrium must be fulfilled for both physical problems. Therefore, the equilibrium equations for the piezoelectric medium are classical equilibrium equations of mechanics and the Gauss' law for electrostatics (which states that the divergence of the electric displacement must be equal to the volume density of free charge):

$$T_{ij|j} + f_i = \varrho\, \ddot{u}_i\,, \tag{1}$$

$$D_{i|i} - q = 0\,. \tag{2}$$

They are, however, perfectly uncoupled equations (i.e., the mechanical and electrical problems do not interfere here).

Similarly, the mathematical model of piezoelectricity adopts invariably the kinematic relations from mechanics (which provides a relationship between the strain and displacement) and the Maxwell's law from electrostatics (which states that the electric field must be curl-free):

$$S_{ij} = \frac{1}{2}(u_{i|j} + u_{j|i})\,, \tag{3}$$

$$E_i = -\varphi_{|i}\,. \tag{4}$$

Here, there is no coupling between both physical problems either.

The coupling occurs in the constitutive equations. Constitutive relations for linear piezoelectricity (in the so-called stress-charge form) are as follows:

$$T_{ij} = c_{ijkl}\,S_{kl} - e_{kij}\,E_k\,, \tag{5}$$

$$D_k = e_{kij}\,S_{ij} + \epsilon_{ki}\,E_i\,. \tag{6}$$

We can easily recognize here the slightly modified Hooke's law for isotropic elastic material. The modification consists in an additional term which comprises the third order tensor $e_{kij}$ containing piezoelectric material constants. A similar term exists in the second constitutive equation where the local electric field is considered to be a function of the material's strain and polarization.

After combination of all the partial differential and constitutive relations we obtain the mechanical displacement versus electric potential equations (presented here for the piezoelectric domain of constant material properties):

$$-\varrho\,\ddot{u}_i + c_{ijkl}\,u_{k|lj} + e_{kij}\,\varphi_{|kj} + f_i = 0\,, \tag{7}$$

$$e_{kij}\,u_{i|kj} - \epsilon_{kj}\,\varphi_{|kj} - q = 0\,. \tag{8}$$

Unknown fields for this problem are mechanical displacements and electric potential ($u_i, \varphi = ?$). They must also fulfil the given boundary conditions; they are:

$$\begin{array}{rccc} & \text{(essential)} & & \text{(natural)} \\ \text{mechanical BC}: & u_i = \bar{u}_i & \text{or} & T_{ij}\,n_j = F_i\,, \\ \text{electric BC}: & \varphi = \bar{\varphi} & \text{or} & D_i\,n_i = -Q\,, \end{array} \tag{9}$$

where:

$\bar{u}_i$ – the specified mechanical displacements,
$F_i$ – the specified surface forces,
$\bar{\varphi}$ – the specified electric potential,
$Q$ – the specified surface charge,
$n_i$ – the outward unit normal vector components.

Obviously, combinations of both types of the boundary conditions are possible. We notice that the boundary conditions are uncoupled and pertain to the unknown mechanical and electrical quantities. In the case of the natural BC we should use again the geometric and constitutive relations to replace $T_{ij}$ and $D_i$ with the explicit expressions for $u_i$, $\varphi$.

## 1.2 Constitutive relations of piezoelectricity

We have shown in the previous Section that piezoelectricity is described mathematically *only* within a material's constitutive equation, which defines how the piezoelectric material's stress ($\boldsymbol{T}$), strain ($\boldsymbol{S}$), charge-density displacement ($\boldsymbol{D}$), and electric field ($\boldsymbol{E}$) interact. We repeat here the piezoelectric constitutive law in the co-called *Stress-Charge form*:

$$\begin{aligned} \boldsymbol{T} &= \boldsymbol{c}_{\boldsymbol{E}=\boldsymbol{0}} \cdot \boldsymbol{S} - \boldsymbol{e}^{\mathrm{T}} \cdot \boldsymbol{E} \,, \\ \boldsymbol{D} &= \boldsymbol{e} \cdot \boldsymbol{S} + \boldsymbol{\epsilon}_{\boldsymbol{S}=\boldsymbol{0}} \cdot \boldsymbol{E} \,. \end{aligned} \tag{10}$$

In these equations, the matrix $\boldsymbol{e}$ contains the piezoelectric coefficients for the material, and it appears twice, while the matrices $\boldsymbol{c}_{\boldsymbol{E}=\boldsymbol{0}}$ and $\boldsymbol{\epsilon}_{\boldsymbol{S}=\boldsymbol{0}}$ contain, respectively: the elastic material constants obtained in the absence of electric field, and the dielectric material constants obtained when there is no strain. The specific subscripts indicates the "field-absence conditions" (we skipped these subscripts in the vector/tensor's components form of constitutive equations presented in the previous Section).

Other forms of piezoelectricity constitutive relations are possible. The four state variables ($\boldsymbol{T}$, $\boldsymbol{S}$, $\boldsymbol{D}$, and $\boldsymbol{E}$) can be rearranged to give an additional three forms for a piezoelectric constitutive equation. Instead of the coupling matrix $\boldsymbol{e}$, they contain the coupling matrices $\boldsymbol{d}$, $\boldsymbol{g}$, or $\boldsymbol{q}$. Obviously, all these forms are equivalent and it is possible to transform piezoelectric constitutive data in one form to another form. These transformations can be quite important since vendors typically publish material data for $\boldsymbol{d}$ and $\boldsymbol{g}$, whereas certain finite element codes require piezoelectric data entered as $\boldsymbol{e}$.

The three remaining possible forms for piezoelectric constitutive equations are shown below. The names for each of the forms is arbitrary; they were taken from the two dependent variables on the left-hand-side of each equation (note that the voltage and electric field variables are gradient-related).

- *Strain-Charge form*:

$$\begin{aligned} \boldsymbol{S} &= \boldsymbol{s}_{\boldsymbol{E}=\boldsymbol{0}} \cdot \boldsymbol{T} + \boldsymbol{d}^{\mathrm{T}} \cdot \boldsymbol{E} \,, \\ \boldsymbol{D} &= \boldsymbol{d} \cdot \boldsymbol{T} + \boldsymbol{\epsilon}_{\boldsymbol{T}=\boldsymbol{0}} \cdot \boldsymbol{E} \,. \end{aligned} \tag{11}$$

- *Strain-Voltage form*:

$$\begin{aligned} \boldsymbol{S} &= \boldsymbol{s}_{\boldsymbol{D}=\boldsymbol{0}} \cdot \boldsymbol{T} + \boldsymbol{g}^{\mathrm{T}} \cdot \boldsymbol{D} \,, \\ \boldsymbol{E} &= -\boldsymbol{g} \cdot \boldsymbol{T} + \boldsymbol{\epsilon}^{-1}_{\boldsymbol{T}=\boldsymbol{0}} \cdot \boldsymbol{D} \,. \end{aligned} \tag{12}$$

- *Stress-Voltage form*:

$$\begin{aligned} \boldsymbol{T} &= \boldsymbol{c}_{\boldsymbol{D}=\boldsymbol{0}} \cdot \boldsymbol{S} - \boldsymbol{q}^{\mathrm{T}} \cdot \boldsymbol{D} \,, \\ \boldsymbol{E} &= -\boldsymbol{q} \cdot \boldsymbol{S} + \boldsymbol{\epsilon}^{-1}_{\boldsymbol{S}=\boldsymbol{0}} \cdot \boldsymbol{D} \,. \end{aligned} \tag{13}$$

The given piezoelectric equations can be readilly integrated in a finite element environnement for instance in order to numerically address a smart piezoelectric component. In the following sections, two possible applications of what is given here are presented. The first application concerns a one dimensional active vibration filtering device. This system was pattented and under industrialisation. The second application concerns active vibration and noise control (AVNC). This is an important context of application of piezoelectric materials, one of possible realisation is dealt with in this paper.

# 2 Smart vibration filtering device

The objective is to cut down on the disturbance generated by a vibrating system in its environment. The passive system under study is a simple rubber mount. Rubber mounts are often used (see Figure 1) in vehicles (or in building) in order to isolate engins (or vibrating machines) and to minimise the solidien disturbances propagation to the habitacle. Their function is mainly a vibration filtration. This filtration occurs in a frequency domain defined by the rubber intrinsic characteristics that depend on their chemical and physical properties. The performances of this system can be improved by the introduction of an active technology. The main originality of this work is the combination of piezoelectric technology with simple rubber mounts abilities. Indeed, the final system is a set of serial connected components which are : the rubber mount, a piezoelectric block of PZT ceramics to generate the command control and finally a PVDF sensor to sense the quantity to be minimized.

It should be adressed, that many other products and solutions are already existing. Indeed, many solutions based on inertia actuators are provided in the marked. Active combined fluid and elastomer mount are also existing, as weel as some solutions using a kind of adaptive damping tuned mass absorber. The solution proposed in this technical note complete this set of strategies and can provide a valuable solution when constraints in terms of weight, consumptions and size are drastic. It should be noted that the additionnal mass in this hybrid piezo-rubber system is reduced to the mass of the piezo-block.

In practice, the rubber mounts abilities to reduce vibration is frequency limited. In fact, unwanted consequent amplification of disturbances will generally happen near the suspension frequency, and saturation and other related phenomenon will also happen at higher frequencies due to the rubber non linearities. The main goal of the present paper is to provide a new design of rubber mounts which uses piezoelectric materials to improve rubber mounts functionnalities.

The hybrid component obtained herein is subject of a simple proptotype. Experimental results are presented showing the performances of the active hybrid rubber mount when an adaptive $x$-filtered LMS law is used. The control

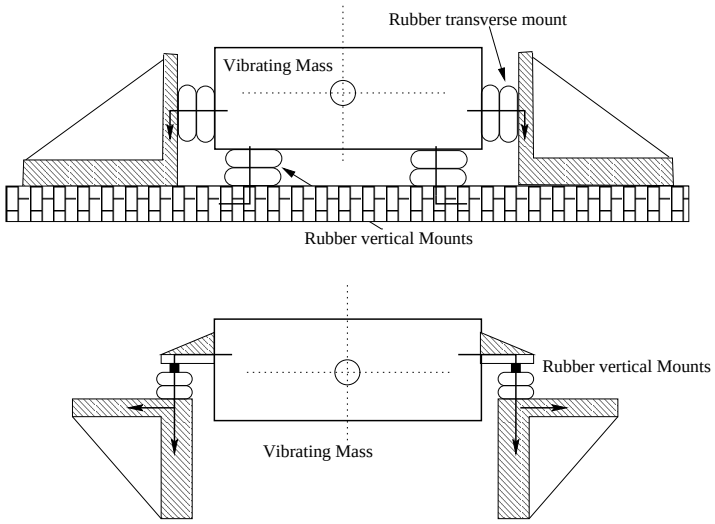


Figure 1: Achievment and mounting of passive rubber mounts

technique implemented in this study does not require a modelisation of the passive system since it's an adaptative one. So identification and control algorithms strategies using transverse or recursive filters and a stochastic gradient resolution method are used.

## 2.1 Experimental mock-up description

The basic configuration of the rubber mount tested here is plotted on Figure 2. This figure shows the different components used in the experimental set-up. An electrodynamic excitator is used as an external perturbation source. The electrical signal that order the excitator is used as a possible reference signal for the standard control system. An impedance head is then employed, the signal delivered will be reffered as force sensor (signal S1) in the remainder text. A 15 Kg mass constituted from a set of 3 steel discs soldered by 2 bolts is introduced to represent the vibrating machine to be isolated. An accelerometer is then used in order to measure mass acceleration signal (designated by S2). This signal will constitute a second possible reference for the controler. The rubber mount used here is a Paulstra one, it is the passive component to improve. A piezoelectric actuator block is a set of 12 patches of 2 mm thickness will insure the actuating command (signal S3). Finally, a force sensor (designated by signal S4) is a simple PVDF sensor which sense the transmitted force. An Acquisition material and signal generator, not shown in Figure 2, as well as a real time card board DSPACE is used to complete the mock-up needs.

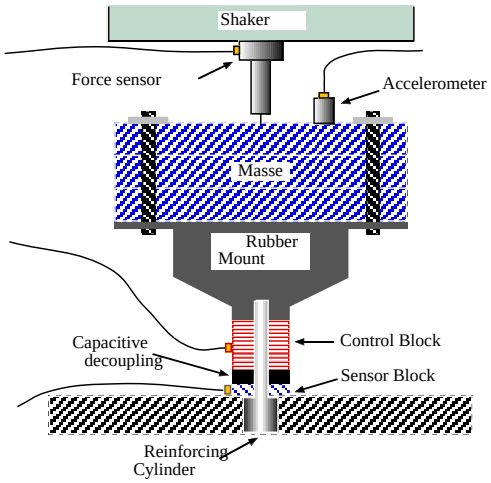


Figure 2: Basic configuration of the rubber mount

## 2.2 Passive responses

In this first measurement part, the electrodynamic excitator is used. The PZT actuator is not ordered any signal in the identification step. The transfer function S4/S1 of the primary path (force at embedding / excitation) is measured by ordering the vibrating excitator a white noise signal in the 0-1600Hz frequency range. This corresponds to the frequency range used for the identification step. The measured transfer function is plotted on Figure (3). The transfer function (S2/S1) is also measured, it connects the acceleration of the mass to the excitation (see Figure 4). Both primary paths can be used in the identification and control steps following the choice of the reference signal. It is however clear that from practical point of view, the the accelermeter signal reference will be prefered.

The transfer function S4/S3 of the secondary path (force at embedding / command) is measured by governing the PZT actuator a white noise signal in the 0-1600Hz frequency range. The electrodynamic excitator is disconnected. The measured transfer function S4/S3 is plotted Figure (5). The transfer function S2/S3 connecting the acceleration of the mass to the command is also plotted (see Figure 6). The secondary path show both resonant and non resonant behaviour. Its right identification using numerical filters will be of dramatic consequences for the control strategy.

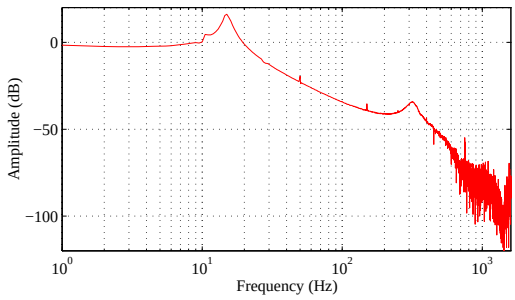


Figure 3: Passive system response : Primary path (Force at embedding/ excitation)

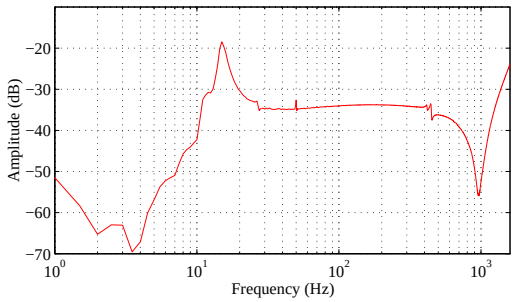


Figure 4: Passive system response (Mass acceleration/ excitation)

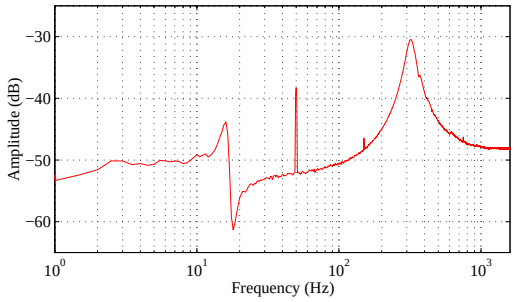


Figure 5: Passive system response : secondary path (Force at embedding/ command control)

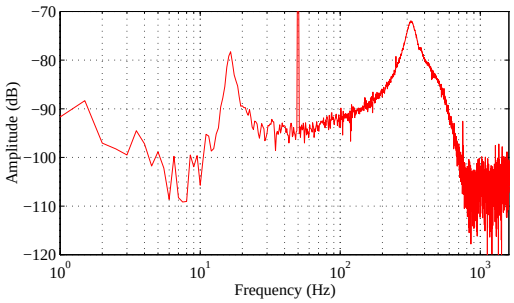


Figure 6: Mass acceleration/ command control)

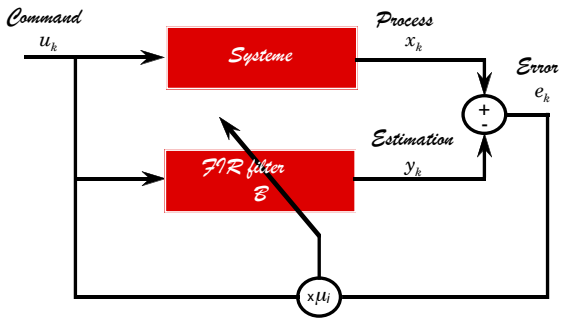


Figure 7: identification filtering scheme: $B_{k+1} = B_k - 2\mu_i e_k U_k$

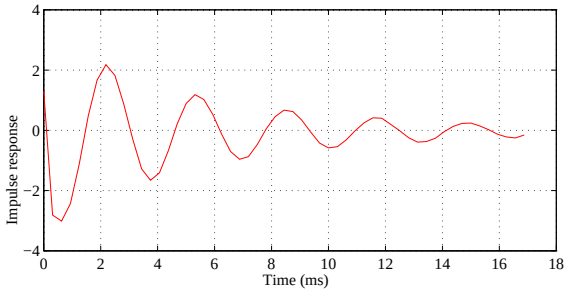


Figure 8: Identification of the secondary path by a FIR of 50 coefficients

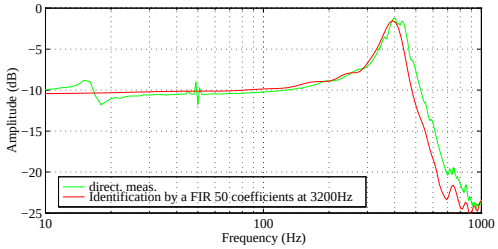


Figure 9: Frequency response of the secondary: comparison between the measurement and the identification of the secondary by a FIR of 50 coefficients

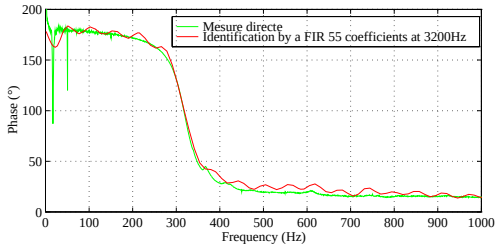


Figure 10: Frequency response of the secondary: comparison between the measurement and the identification of the secondary by a FIR of 50 coefficients

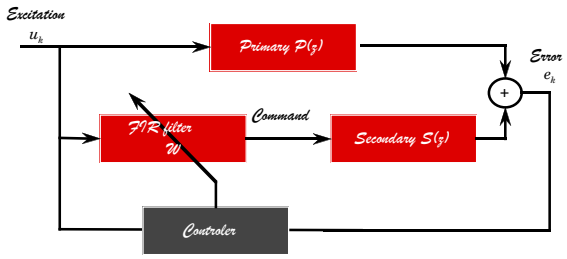


Figure 11: control filtering scheme

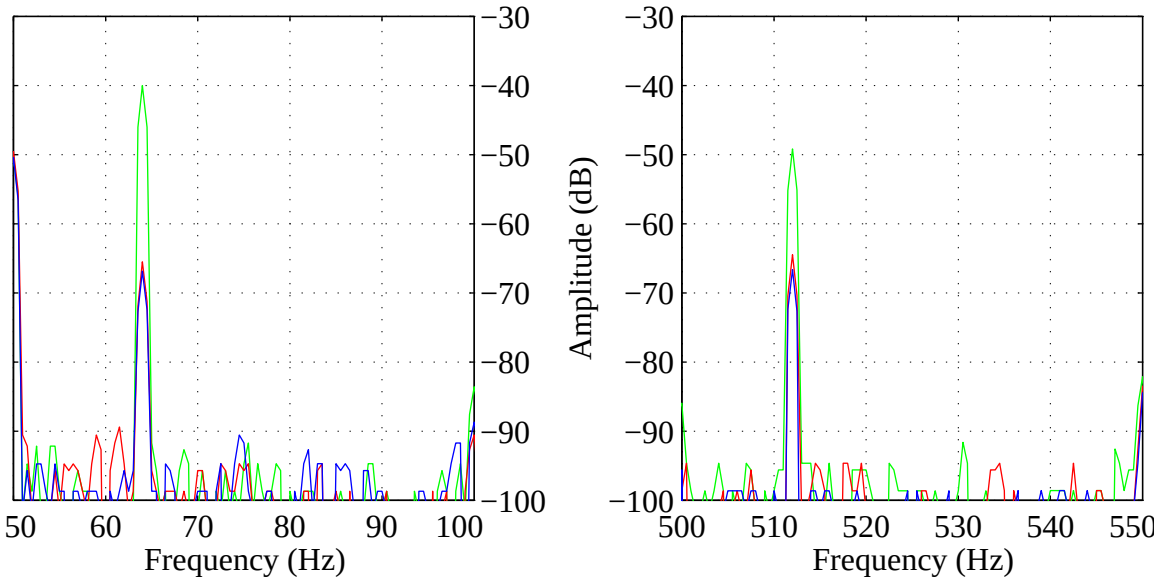


Figure 12: Force at embedding : active versus passive results for frequency lines 64Hz and 512Hz

## 2.3 Secondary path identification

Figure (8) gives the identification results of the secondary path by a FIR [1, 2, 3, 4, 5] of 50 coefficients (see Figure 7). The impulse response of the secondary is rather short (about 15ms). Figures (9) and (10) gives the frequency response of the measured secondary path and the identified FIR filter. Both amplitude and phase results are plotted. The agreement between the two curves is rather good since the very low frequencies until 500 Hz-600 Hz. So the controler should be carried out under good conditions on this frequency range. Beyond 600 Hz, the disagreement in amplitude and phase of the filter will limit the performances and the stability of control [2, 4].

## 2.4 Control results

Active versus passive performances of the hybrid rubber mount are plotted Figures (12, 13, 14, 15). The control technique used here is the classical x filtered LMS (see Figure 11) , [2, 4]. This control law was implemented under Simulink package and using the DSPACE tools and facilities. The controlled rubber mount frequency range is limited by two phenomenon: For high frequencies, beyond a certain sampling frequency of the signals, the control algorithm does not converge. For low frequencies, it is the actuator delivered power which limits the control performances. In fact, piezoelectric actuators

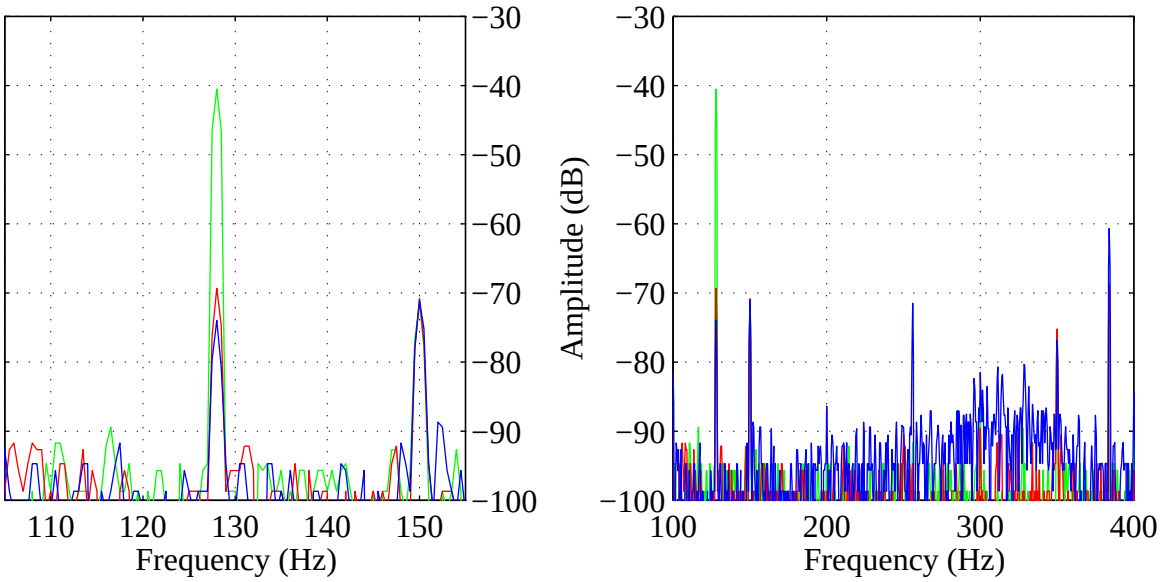


Figure 13: Force at embedding : active versus passive results for frequency line 128Hz The use of two scales highlights the noise rejection at high frequencies by the acceleration control

are command tension limited (around 1000 V/mm) and are thus well suited for high frequency active isolation. For the considered rubber mount, the frequency range of control is placed in the neighbourhoods of the interval 50Hz-700Hz. Figure (12) compares the measurement of the force at the embedding of the passive and the active mount, for two harmonic excitations. It clearly shows the effectiveness of the active insulation of the excited frequency, even the control tends to increase the noise level at low frequencies near the frequncy line 64Hz.

The gain obtained on the frequency line by the adaptive control is approximately 15 dB for 640 Hz and of 25 dB for 64Hz. Between these two extreme values of the frequency, the insulation by the active mount is about 20 dB. Parallel to profit which believes when the frequency decreases, At low frequencies the control gains increases. The power necessary to control increases too: it is noted that it is $10^4$ times greater when the frequency passes from 640 to 64Hz!. This strong power necessary to control can explain the increase in the noise noted during the insulation of the line 64Hz. If the actuator work away from its linear operating conditions (saturation of the feeding), the estimation of the secondary by the filter is not yet correct, and can generates an additional noise.

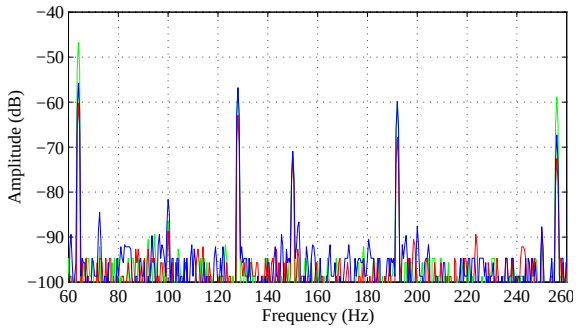


Figure 14: Force at embedding : active versus passive results for 4 frequency lines 64, 128, 196, 256 Hz

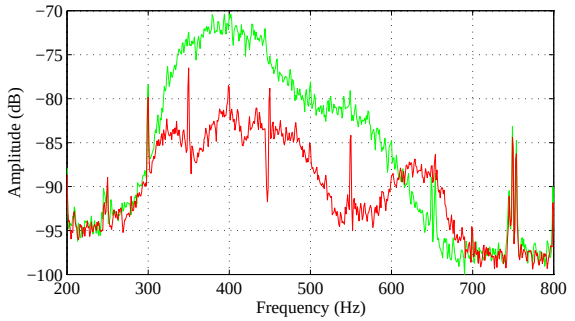


Figure 15: Force at embedding : active versus passive results for a white noise 400-600Hz

### 2.5 Conclusions

In this section, a new concept of hybrid rubber mount is reported. This concept tends to validate a very simple and attractive idea consisting on the adjonction of a piezoelectric bloc to the passive rubber mount in order to extand its frequency range effeciency and to improve its vibration filtering pecularities over a wide frequency range. The concept proposed here was validate and proved the interest of such technique. Almost 10 average dB improvement was achieved for a white noise rejection. It should be adressed also that the additional cost relative to control algorithm and devices is relatively limited with regards to the performance and the added value of the hybrid component.

## 3 Smart structures through piezoelectric materials

Nowadays, the active vibration and noise control (AVNC) devices are studied and integrated more often at the design stage of new products and equipments. (AVNC) devices when added to intrinsic passives capabilities can offer considerable improvement in the product services. Among such product, the double panel partition have known an extraordinary interest from the active noise control community. The great number of journal or congress papers addressing this very particular [6, 7, 8] example prove the industrial interest on double panel partition.

In fact, The double panel partitions are often used in noise control engineering thanks to their high attenuation capacity of noise and their low weight. Double panel are for instance used as double glazing windows, aircraft fuselage or in some car bodies. In practice, double panels are used when lightweight structures with high insertion loss are desirable. However, the performances towards lower frequencies rapidly deteriorates to even fall short of a single panel. At low frequencies, indeed, the transmission loss is mainly dominated by the double wall resonant effects. For idealized infinite double panels with an air gap, a simple theoretical computation clarify better the situation. In fact, theoretical computation leads to the well known [9] mass-air-mass frequency associated an opposite phase rigid panels motion ("the swelling mode shape").

To improve the sound reduction counteracting intrinsic double panels phenomenon, several active control strategies have been investigated, simulated and often experimentally verified as reported in references [8, 10, 11], showing the effectiveness of active solutions. However researches are still in progress to find some easy ways of control. Unlike usual proposed solutions [10], the work

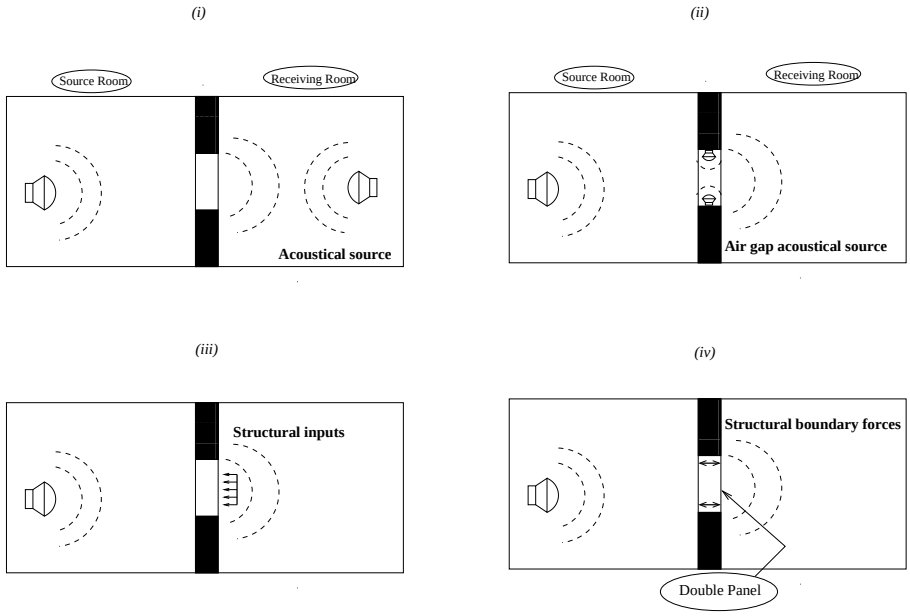


Figure 16: Classification of possible control strategies: *(i)* active acoustical control in the receiving room; *(ii)* air gap active acoustical control; *(iii)* structural inputs to the radiating panel and *(iv)* structural inputs at the double panel boundaries

reported here *concern a pure structural vibration strategy.* Further strategies in the control of sound transmission through flexible panels or double panels into an enclosure are discussed in references [12, 13].

Since the earlier patented work, from the authors knowledge, due to Gargliardinni *et al.* [10], a great number of papers dealing with the activation of double panel partition have been published. Following, Gagliardinni's original work, the majority of published papers propose acoustical active treatments of the problem. Among those papers let us mention the work published by Bao and his colleagues [6, 14]. In [6], for instance, a classification of acoustic strategies is proposed. Authors distinguish three main ways to improve insertion loss of double partitions. Actually, the control can be achieved using:• an acoustic source placed in the receiving room, • an active structural acoustic thanks to injected secondary forces directly to the radiating panels, • or finally an acoustic source in the air gap between the panels (see Figure 16).

Those three ways seem to be the most studied ones in the literature. Many comments can be drawn from this review. In fact, the first strategy using directly a secondary acoustical source in the receiving room is a common solution proposed a long time ago. However, from the authors point of view, it cannot be considered as an intrinsic strategy to improve the transmission loss of double panel. This control strategy is obviously based on the measured

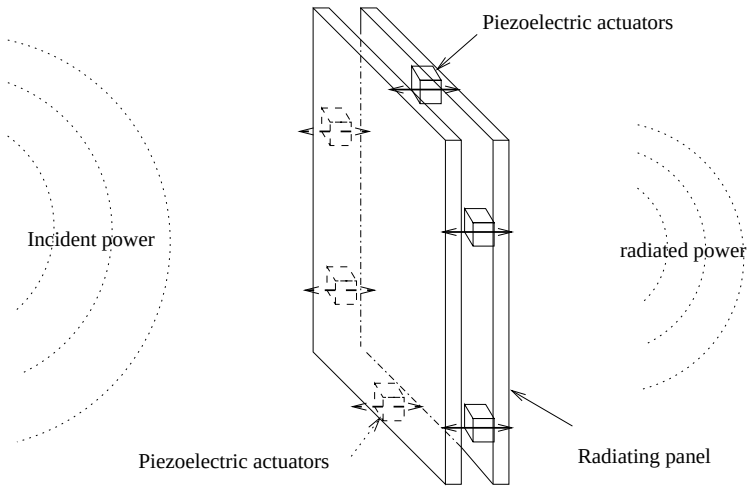


Figure 17: Proposed boundary structural control

sound pressure level in the receiving room which represents the global sound level due to multiple transmission mechanism. The third way to enhance the transmission loss, [10, 11], seems to be the most studied one in the literature. Gargliardinni *et al* [10] compares this strategy to sophisticated passive double glazing window. In particular, he shows that similar active/passive results can be obtained when using passively an Helium gas in the cavity gap between panels.

The solution proposed in this paper can be ranked among the second class of active double panel strategies. In this case, as explained before, structural control inputs are used rather than acoustical ones. A considerable amount of works have been published in the context of structural control of radiating sound. Structural input forces are applied to the vibrating structure in order to minimize the sound radiation. This idea can be used for the double panel case, using either piezoelectric patches glued on the structure, or punctual vibration absorbers correctly tuned to the structural dynamics. Carneal [15], for example, shows that the use of vibration inputs is suited to reduce the transmission loss. The differences between structural and cavity control were investigated by Bao and his colleagues [14] and also by Gardonio [16]. Control laws used for either structural or acoustical double panel control are of feedback [6] or feedforward [10] kind.

The idea defended in this section (see Figure 17) is an original and easy way to improve transmission loss of a double panel partition. As an immediate application, a double glazing window is under study. The control strategy principle is to use a further structural path of motion between the panels. As shown in (Figure 16), for some realistic double glazing windows, there exist two kinds of coupling mechanism between panels: the air gap coupling

and the structural boundary coupling. The combination of both coupling ways leads to transmission loss deterioration at low frequencies. Therefore, "the swelling mode shape" will depends on the global stiffness of the air gap plus boundaries. In fact, in the acoustic cavity control, only the contribution of the air gap is dealt with. *The double panel control strategy proposed in this contribution acts directly on the contribution of the boundary stiffness to improve the transmission loss at low frequencies* (see Figure 17).

Hence, the paper starts by a general presentation of the realistic double glazing window under numerical study and experiments. In this context, both the experimental set-up which is employed for the active idea validation, and the corresponding numerical model established in view of vibroacoustic behavior better understanding, are detailed in section 3 of this paper. Notably, the insertion loss index used for the qualification of the vibroacoustic performances of a double panel partitions is briefly presented. This criterion is combined with a precise finite element modeling of the experimental set-up and permits a parametric survey to be conducted. Tools proposed in section 3 are in fact employed for the passive double glazing window behavior analysis. Results are presented and deeply commented in section 4. In fact, the air cavity and the boundaries characteristics influence on the insertion loss is studied thanks to the finite element modeling. This parametric survey reveals that the boundaries stiffness affect the insertion loss behavior. Ultimately, free modes of the double glazing windows contributing to the sound reduction decay are identified. Ultimately, an experimental set-up of the active device based on a structural boundary active strategy is proposed. The later is well convenient for practical double glazing applications. Comparisons between measurements and numerical computation is proposed as well as control results and performances.

## 3.1 Double panels partition under study and experiments

In this section, the analyzed double glazing window is described. The structural complexity of the problem push away pure analytical modeling. Such analytical descriptions are, practically, limited to *non realistic double glazing windows*. In this work, a complete finite element modeling of the realistic configuration is proposed. This is a structural-acoustical coupled model which leads to some basic phenomenon understanding. Notably, this numerical modeling will be used later for a parametric survey of the passive system. It allows also numerical computation of the sound transmission loss reusing the pure structural finite element results.

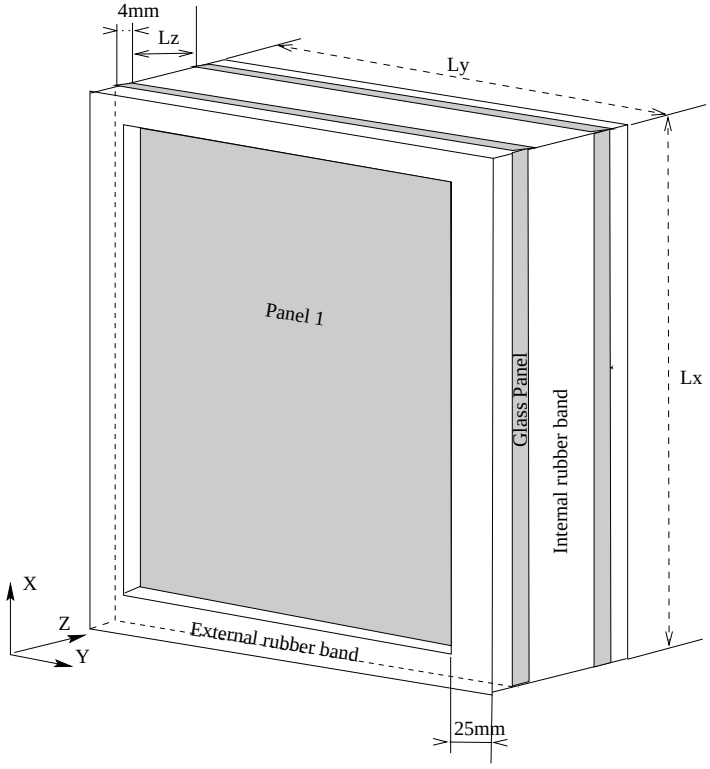


Figure 18: Double panel partition set-up

### 3.1.1 Description of the studied realistic double panel partition

The double panel partition consists of two identical flat and rectangular glass panels, maintained together to a rigid body by a two $3\,mm$ thick rubber bands. A third $12\,mm$ thick rubber band is used as shown in (Figure 18), as an internal joint between the panels. The free dimensions of each panels are $800\,mm \times 600\,mm \times 4\,mm$. It should be noted that dimensions used in this investigation are standard as well as the mounting configuration of the system. This system contains structural and fluid elements which obviously interact.

In the experimental analysis, two distinguish perturbations of the double glazing window was used in view of system identification and control. Precisely, a pure acoustical source is used thanks to a loudspeaker placed at a $1500\,mm$ from the system incident panel. An impact hammer is also employed as a structural source. Two accelerometers bonded onto the radiating panel are used in both the identification and the control steps of the dynamical behavior of the double panel partition. The impact hammer technique is used to identify the mode shapes of both panels. Ultimately, two microphones

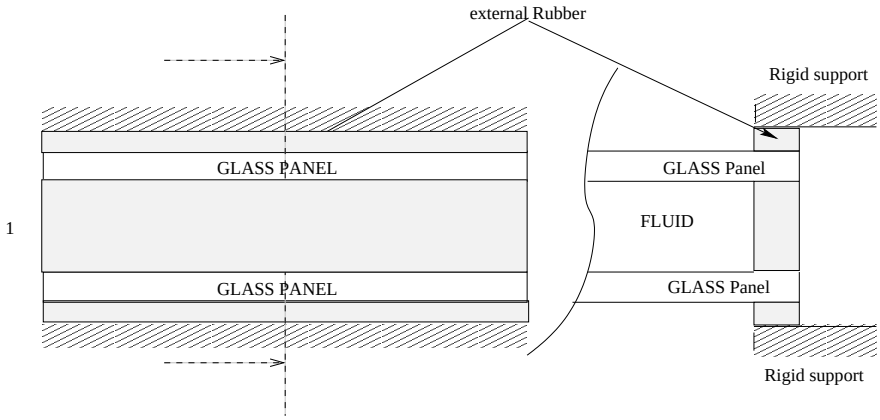


Figure 19: Finite element modeling of the full scale double panel partition.

are used in this experimental set-up. The first acoustical microphone is placed in the air gap cavity, it provides measurements of the acoustical pressure variations in the cavity. The second microphone placed in the receiving free space (at $1.5\,m$ far from the radiating panel) gives measurement of the free radiated pressure.

### 3.1.2 Finite element modeling of the double panels

A 3D full scale finite element modeling of the experimental set-up was first performed. This model was realized using ANSYS finite element code. Both structural and acoustical elements was considered. Particularly, glass panel was modeled using elastic shell elements. External as well as internal rubber interfaces was represented using 3D elastic shell distribution along edges of the system. This was done using intrinsic pure stiffness elements from ANSYS library. Stiffness values was estimated using equivalent quasi-static experimental set-up. Boundary conditions for the model corresponds to those represented in (Figure 19).

Ultimately, the internal bounded fluid was introduced. Two kinds of elements was considered: • fluid elements in contact with the structural glass, which provides a full representation of the fluid-structure interaction and • Pure fluid elements for the internal cavity modeling. Both free and forced linear simulations was performed thanks to the full scale finite element model. In fact, a modal analysis of the experimental set-up as well as the system response to a forced pressure distribution applied to the emitting glass was done. Structural responses (velocity of the receiving glass panel mainly) was used as explained in the subsequent text in order to compute numerically the transmission loss factor of the equipment.

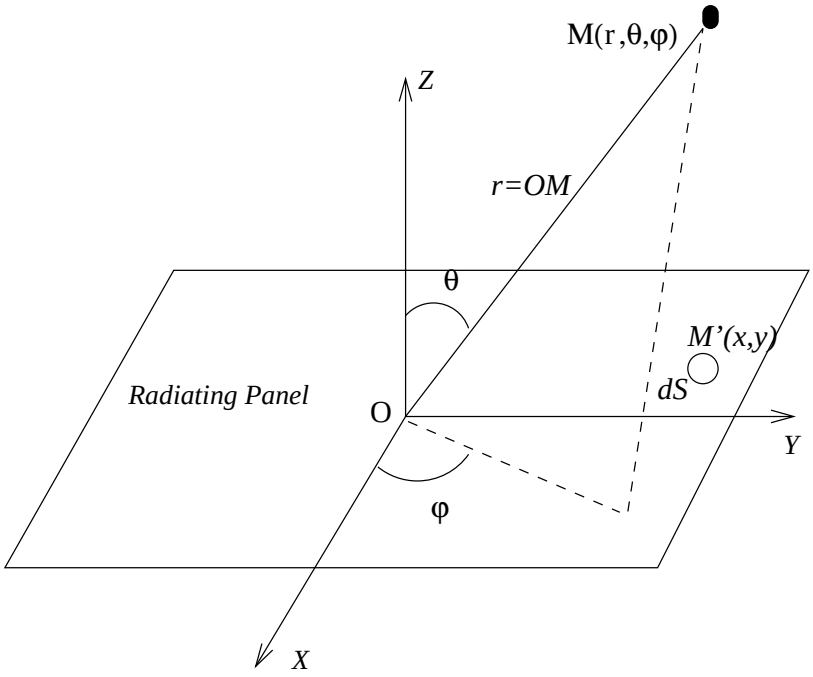


Figure 20: Radiating panel

### 3.1.3 Transmission loss computation

This section briefly defines the computation performed through finite element modeling. The overall objective is to analyze the structural and acoustical influence on the vibroacoustic performances of the double panel partition. the panels dimensions are designated by $L_x$, $L_y$ in the following, $L_z$ being the width of the fluid cavity. Let the Sound Reduction Factor be the ratio of the radiated acoustic power $P_{rad}$ (acoustic radiated power in a half space limited by the infinite baffled double panel partition) by the double panel partition of the incident acoustic power $P_{inc}$:

$$R = log_{10}(\frac{P_{inc}}{P_{rad}}) \tag{14}$$

Using the notations of Figure (20), the radiated power $P_{rad}$ can be simply given by expression (15) as:

$$P_{rad}(\omega) = \int_0^{2\pi} \int_0^{\pi/2} \frac{|p(r,\theta,\phi,\omega)|^2}{2\rho_f c_f} . r^2 \sin(\theta) d\theta d\phi \tag{15}$$

Where $\rho_f$, $c_f$ are acoustic fluid density and celerity respectively. $(r,\theta,\phi)$ represents the spherical coordinates system employed here. $\omega$ being the excitation frequency and $p(r,\theta,\phi,\omega)$ the pressure at the listening point $M(r,\theta,\phi)$. The

| | Young modulus$Pa$ | Density $\rho$ $kgm^{-3}$ | Poisson's ratio $\nu$ | Celerity $ms^{-1}$ |
|---|---|---|---|---|
| Glass | 60 $10^{10}$ | 2480 | 0.3 | – |
| Rubber | 9.89 $10^{6}$ | 1495 | 0.45 | – |
| Fluid (air) | – | 1.29 | – | 340 |

Table 1: Elastic and acoustic constants of the double panel elements

later is given in expression (16) which is the Rayleigh integral representing the far field pressure profile:

$$p(r,\theta,\phi,\omega) = -\rho_f \int_{S_p} \frac{e^{-ikM'M}}{2\pi M'M}\omega^2 w(x,y,\omega)dS \tag{16}$$

$M'(x,y,0)$ is the center of the radiating elementary surface $dS$ in Cartesian coordinates. Where $w(x,y,\omega)$ designates the flexural displacement of the radiating panel measured at point $M'(x,y)$ and $S_p$ is the integration area on the radiating panel. Finally, $k$ is the acoustic wave-number. To compute the radiated pressure $p(r,\theta,\phi,\omega)$ it is assumed that: • Firstly the output point $M$ is located in the far field. In this case, one can write the following approximation. $M'M = r - \sin(\theta).(x\cos(\phi)+y\sin(\phi))$ if $(r >> L_x, L_y)$. Hence the equation (16) is transformed into the following equation (17):

$$p(r,\theta,\phi,\omega) = -\rho_f \frac{e^{-ikr}}{2\pi r} \int_{S_p} \omega^2\, w(x,y,\omega).^{(j\frac{\omega}{c_f}\sin\theta(x\cos\phi+y\sin\phi))} dxdy \tag{17}$$

• Secondly the flexural displacement $w(x,y,\omega)$ is considered to be a weighted linear combination of modal quantities (see expression (18)):

$$w(x,y,\omega) = \sum_{k=1}^{m} q_k(\omega)\phi_k(x,y) \tag{18}$$

$q_k$ being the $k^{th}$ modal participation factor. Functions $\phi_k$ are the modal shapes of the structure which are performed by a modal finite element analysis of the double panel partition.

In this analysis, the elastic constants of the experimental set-up components (glazing panels, rubbers and fluid) reported in Table (1), are used. as explained before, Shell elements for the panels, three dimensional acoustic fluid elements for the fluid cavity and three dimensional solid elements for rubber band are also used.

In the case of light structural damping, the Basile's hypothesis can be used [17], so that the governing equation of the modal coordinate $q_k$ can be given

by Equation:

$$\ddot{q_k} + 2\xi_k\omega_k\dot{q_k} + \omega_k^2 q_k = \int_{S_p} F_{inc}\phi_k dS = f_{inc}^k \tag{19}$$

or likewise,

$$q_k(\omega) = \frac{f_{inc}^k}{\omega_k^2 - \omega^2 + 2j\xi_k\omega_k\omega} \tag{20}$$

$F_{inc}$ being the external force distribution due to the incident pressure. $\xi_k$ being the equivalent modal damping factor. If expression giving (20) the modal coordinate $q_k$ is combined with expression (18), then the pressure profile expression given at first in (17), becomes (21):

$$p(r,\theta,\phi,\omega) = S^T(r,\theta,\phi,\omega)Q(\omega) \tag{21}$$

where the entities $S$ and $Q$ are vector quantities such that: $S^t(r,\theta,\phi,\omega) = [S_1, ...S_N]$ and $Q(\omega) = [q_1, ...q_N]^t$ with:

$$S_k(r,\theta,\phi,\omega) = -\rho_f \frac{e^{-ikr}}{2\pi r} \int_{S_p} \omega^2\phi_k . ^{j\frac{\omega}{c_f}\sin\theta(x\cos\phi + y\sin\phi)} dxdy \tag{22}$$

Now, the radiated power is obtained readily by the following equation :

$$P_{rad}(\omega) = Q^t(S^tS)Q \tag{23}$$

Hence, the sound radiation factor is computed numerically from a finite element modeling of the realistic double panel partitions. Parametric survey can thus be achieved in order to appreciate the influence of the acoustical and the structural components on the overall performances of the double panel. In the following section, an analysis of the vibroacoustic performances of the double glazing window is proposed. In particular, the air gap cavity and the boundary stiffness incidence on the transmission loss are analyzed.

## 3.2 Analysis of the passive double panel partition

This section is mainly devoted to the insight of major sound transmission mechanism of the passive double panel. To this end, the numerical model established in the previous section will be employed. Some results will be experimentally checked. This numerical model will also be extensively employed in view of a parametric numerical study. This parametric survey includes mainly an analysis about the contribution of the boundary stiffness to the sound transmission factor.

| Structure and no fluid | | | Structure with fluid | | |
|---|---|---|---|---|---|
| frequency (Hz) | phase | eigenform $\phi^*_{i,j}$ | frequency (Hz) | phase | eigenform $\phi^*_{i,j}$ |
| 69 | + | (1,1) | 69 | + | (1,1) |
| 71 | - | (1,1) | 89 | - | (2,1) |
| 118 | + | (2,1) | 118 | + | (2,1) |
| 120.5 | - | (2,1) | 139 | + | (1,2) |
| 165 | + | (1,2) | 154 | - | (1,1) |
| 168 | - | (1,2) | 165 | - | (1,2) |
| 199 | + | (3,1) | 189 | - | (2,2) |
| 203 | - | (3,1) | 199 | + | (3,1) |
| 211 | + | (2,2) | 211 | + | (2,2) |
| 215 | - | (2,2) | 227 | - | (3,1) |
| 288 | + | (3,2) | 254 | - | (3,1) - ! |
| 293 | - | (3,2) | 266 | - | (3,2) |

Table 2: Modal shapes and frequencies of the structure without and with internal fluid.

### 3.2.1 Fluid cavity effects

Only numerical finite element analysis is performed here to understand the effects of the fluid cavity on the modal behavior of the double panel partition. Physical characteristics given in Table (1) are used here. So, a first modal computation of the double partition was performed without internal fluid cavity. As shown in Table (2), this computation leads to a set of modes organized by pairs. For each mode of a given pair, the two panels have the same shape. However, for the first mode, the two panels move in phase and for the second the panels move out of phase (the sign + is assigned to in phase motion of the panels, the sign − to the out of phase motion). Their resonance frequencies are close each to other.

Now if the partition is taken with its structural and acoustical elements, the arrangement of modes changes because of the fluid-structure interaction (see Table (2)). Precisely, the later makes known that the resonance frequency of a mode where the panels move in phase is close to the resonance frequency of the same mode of the system without the fluid cavity. This is an indication of the weak coupling between structural and acoustical subsystems. However, The resonance frequency of a mode where the panels move out of phase is either lower or higher because of the added mass or the added stiffness du to the fluid-structure contribution.

| fréquency en Hz | phase | shape $\phi^*_{i,j}$ |
|---|---|---|
| 63 | + | (1,1) |
| 104 | - | (2,1) |
| 122 | + | (2,1) |
| 145 | + | (1,2) |
| 161 | - | (1,1) |
| 173 | - | (1,2) |
| 203 | + | (2,2) |
| 216 | - | (2,2) |
| 239 | - | (3,1) |
| 266 | - | (3,2) |

Table 3: Measured modes of the experimental set-up

For instance, mode (2,1) (which is an 'out of phase' mode) illustrates clearly the added mass contribution. Indeed, its frequency moves from $f = 89\,Hz$ (with internal fluid) to $f = 120.5\,Hz$ if fluid is not considered. Thus, the fluid has in fact a transversal motion which generates kinetic energy decreasing consequently the resonance frequency from $120.5\,Hz$ to $89\,Hz$. The second example of an 'out of phase' mode (1,1) illustrates the stiffness loading effects of the fluid. Actually, this mode occurs at the resonance frequency $f = 154\,Hz$ if the fluid is considered in the partition but occurs at $71\,Hz$ without internal fluid. Here, the fluid works clearly as a spring introducing a rigidity effect.

## 3.3 Model identification

An experimental identification of the passive system was conducted. Modal testing was operated using impact hammer technique. Hence, the modal shapes and frequencies of modes in the frequency range $0 - 400Hz$ are identified and reported in Table (3). In this table, the signs "+" and "-" in the column "phase" indicate respectively that the panels move in phase and out of phase. In the "eigenfunctions" column, the numbers of the couple (m,n) indicate the half wave-number respectively in the X and Y directions of the panel. The comparison between these modes and those obtained from the finite element analysis shows the same order of the modes but a slight difference on the resonance frequency is noticed because of errors on rubber rigidity values.

To identify radiating modes on the experimental set-up, an acoustical test is realized in free space at $1.5\,m$ far from the double panel partition and the measured radiated pressure is represented in Figure (21).

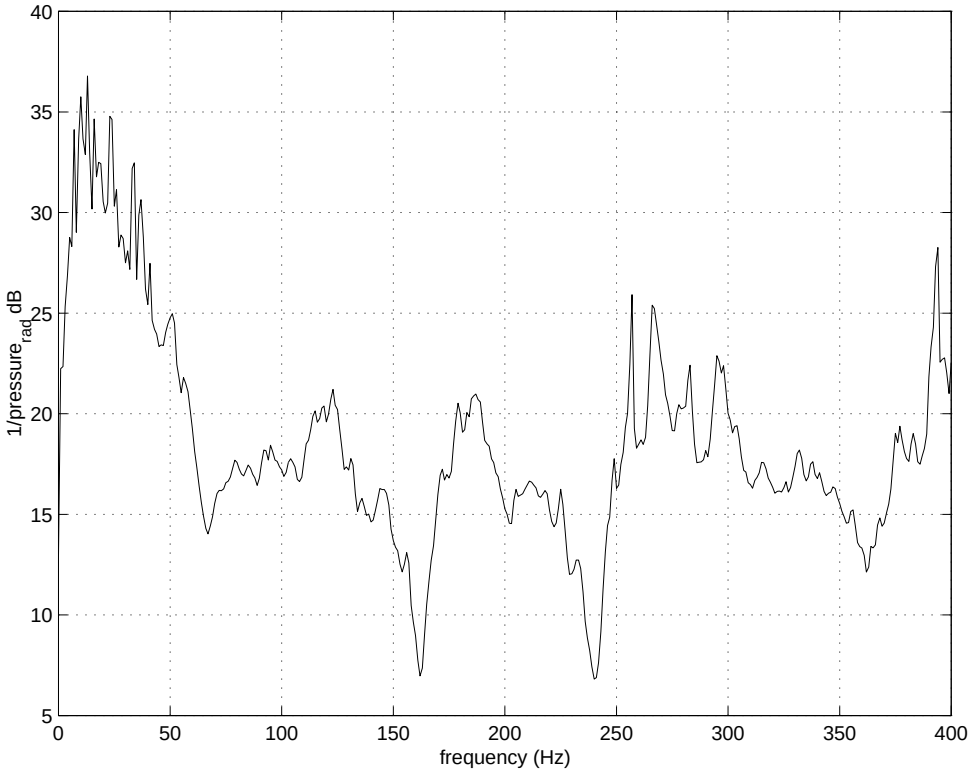


Figure 21: Measured radiated pressure

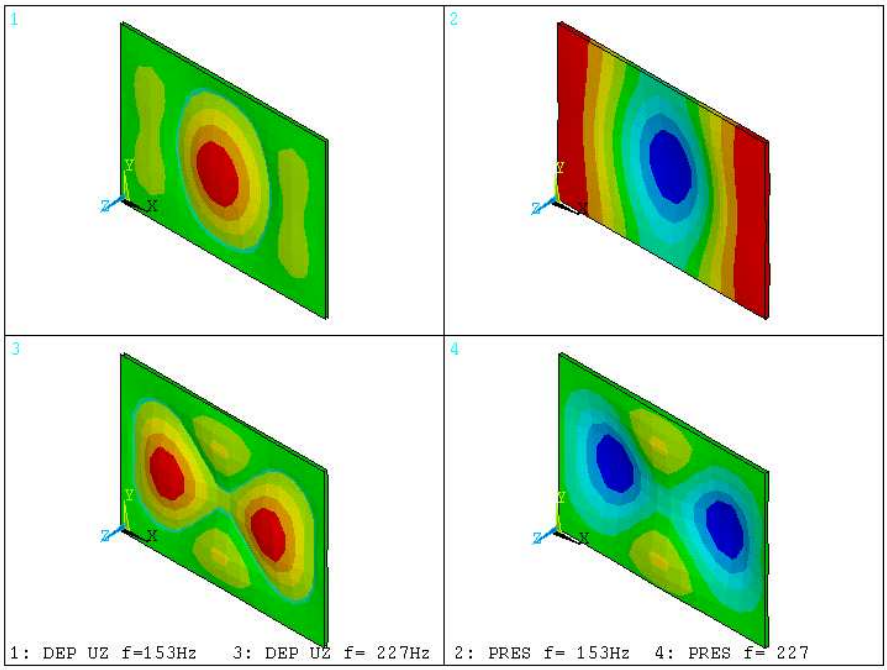


Figure 22: Shapes of the radiating modes: (1) and (3) flexural displacement - (1) and (3) internal pressure for $f_1 = 153\,Hz$ and $f_3 = 227\,Hz$.

| Finite Element Calculus | | | Experimental identification | | |
|---|---|---|---|---|---|
| frequency (Hz) | phase | eigenform $\phi^*_{i,j}$ | frequency (Hz) | phase | eigenform $\phi^*_{i,j}$ |
| 154 | - | (1,1) | 161 | - | (1,1) |
| 227 | - | (3,1) | 239 | - | (3,1) |

Table 4: Identified radiating modes

Such acoustical test was realized in "slightly" a free space because of the lack of an anechoic room. The result given in Figure (21) is similar to the one obtained by the finite element calculus. Unfortunately, experimental and numerical results cannot be compared directly as the acoustical numerical and experimental conditions are not completly the same. However, raisonnable global behavior of both experimental pressure (Figure 21) and numerical one (Figure 23), can be observed. It should be noticed that the level of the transmitted power of the second and the third resonance, as indicated in Figure (21), is almost $7\,dB$ more important than the remaining peaks. Only these two associated modes will be kept for the control process definition. Their shapes identified experimentally, are identical to modal shapes given from the finite element computation shown in Figure (22).

| Configuration | Config. 1 | Config. 2 | Config. 3 |
|---|---|---|---|
| External Rubber ($E_{ext}$,$Pa$) | $10^4$ | 2 $10^5$ | 9.89 $10^6$ |
| internal Rubber ($E_{int}$, $Pa$) | $10^4$ | 2 $10^5$ | $10^6$ |

Table 5: Simulated configuration

In Table (4) are reported the numerical and experimental modal shapes and frequencies of the identified radiating modes.

## 3.4 Boundaries effects on the sound transmission factor: parametric study

In this subsection, results extracted from finite element and transmission loss computations are reported. Table (5) summarizes three configurations of the double panel partitions that are used in view of a parametric study. Only the elastic constants of the three rubber bands (external and internal boundaries of glass panels) are taken as variable. Configuration denoted 3 here is the realistic experimentally tested double glazing. The remaining parameters are hold similar to those given in table (1). In Figures (23) and (24), the sound transmission loss associated with configuration 1 and 2 respectively are represented. Each curve shows one significant peak which corresponds to the so-called mass-air-mass or swelling mode.

Such phenomenon is well known in the double panel vibroacoustic behavior (see for instance [9]). In fact, if the ideal case of infinite double panel partition is considered, one can easily show that this mode corresponds to a high decay of the transmission loss and it corresponds to an out of phase moving panels (assimilated here to rigid masses). Around the frequency of such a mode, the infinite system behaves as a mass-stiffness-mass system of Figure (25). Its frequency is given simply by (24).

$$f_{mam} = \frac{1}{2\pi}\sqrt{2.K_{air}(\frac{1}{M_1} + \frac{1}{M_2})} \tag{24}$$

where $K_{air} = \frac{\rho_f c_f^2}{L_z}$ describes the equivalent air rigidity per unit area, and $M_1$, $M_2$ are mass per unit area respectively of emitting and receiving panels (here $M_1 = M_2$). In the realistic case considered in this study, the external and internal rubber bands introduce stiffness (see Figure (26)) that slightly affect the mass-air-mass mode frequencies. Precisely, in the case of lower rubber stiffness ($K_{air} > K_{int}, K_{ext}$) and considering that $M1 = M2$, equation (24)

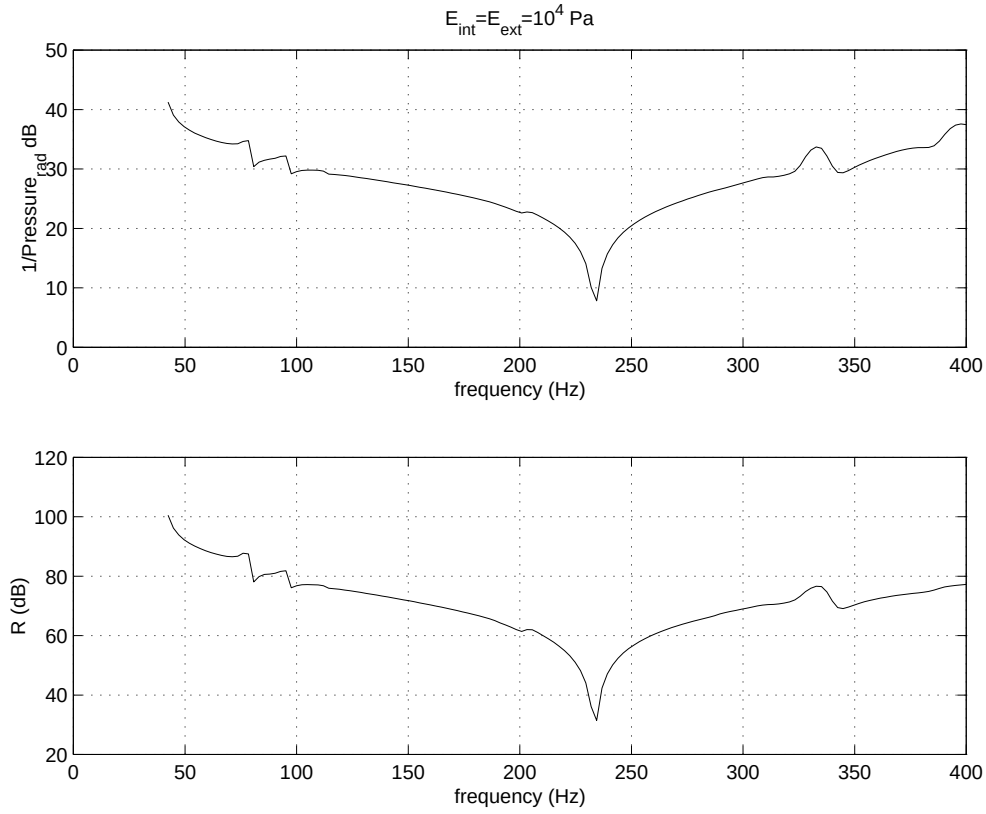


Figure 23: Radiated power in configuration 1.

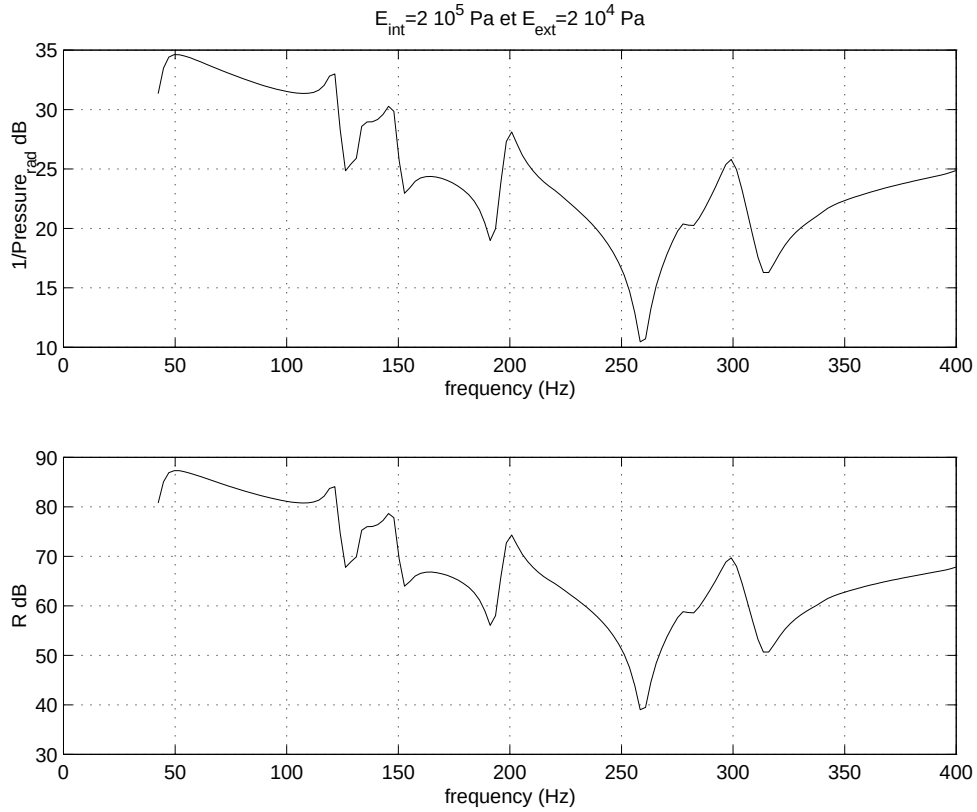


Figure 24: Radiated power in configuration 2.

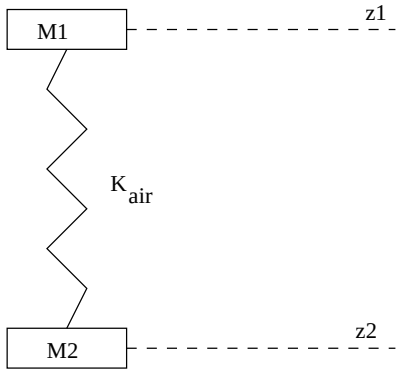


Figure 25: Ideal mass-air-mass system

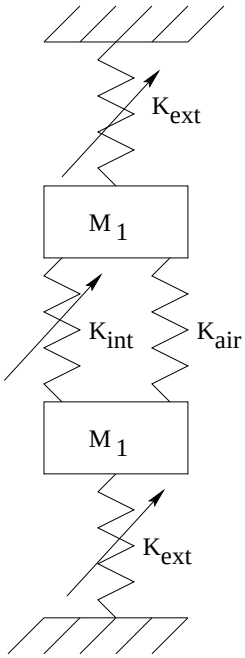


Figure 26: Realistic mass-air-mass system

becomes:

$$f_{mam} = \sqrt{\frac{2(K_{air} + K_{int}) + K_{ext}}{M_1}} \tag{25}$$

where $K_{int}$ and $K_{ext}$ are the rigidity of internal ad external rubber bands respectively. The transmission loss given in Figure (27) shows more than one resonant peak. The mass-air-mass mode notion is not yet valid in the associated configuration (config.3 here). In fact, the rubber stiffness in this configuration is comparable to the fluid equivalent stiffness. So that, the system becomes globally more rigid and more than one mode appear in the corresponding frequency-range. It should be noted that much higher rubber stiffness leads to a single panel behaving system where its mass is the sum of the two panel masses. Ultimately, in all simulated configurations, peaks shown in the transmission loss correspond to symmetric and panels out of phase modes.

## 3.5 Active control of the double glazing window

As seen in the previous section, the boundaries rigidity affects notably the transmission loss. The control process chosen will thus take action directly on this contribution. So, in view of controlling both radiating modes $(1, 1)$ and $(3, 1)$, piezoceramic actuators are employed. Their locations is first optimized

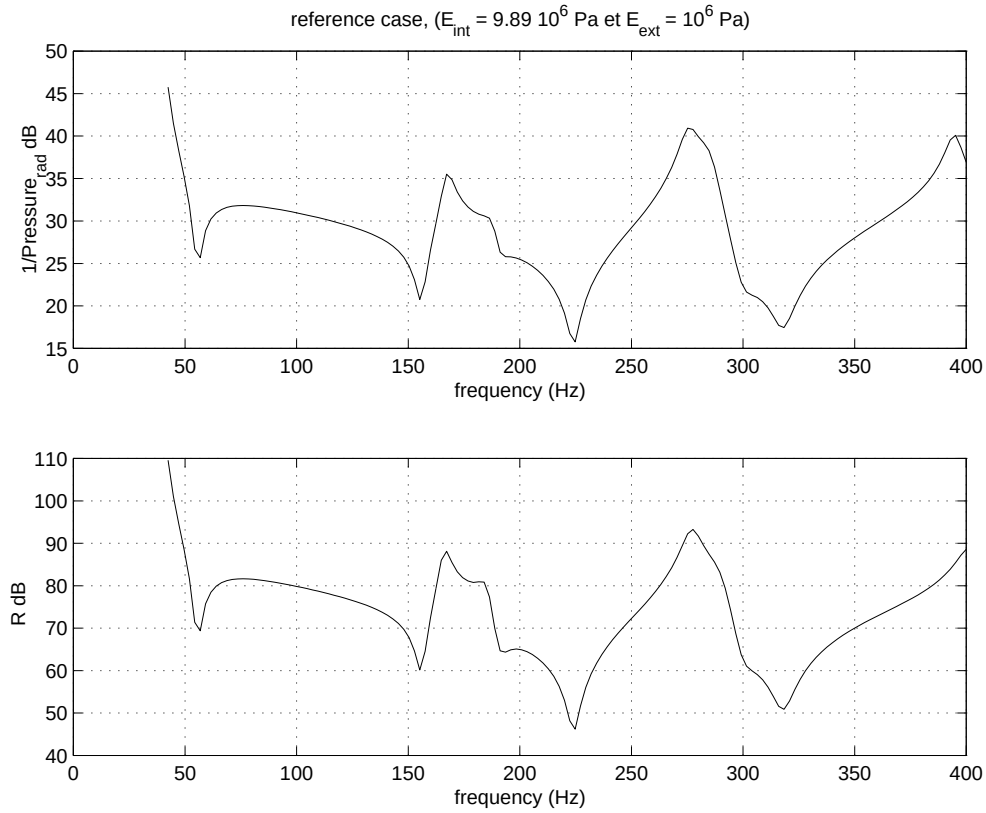


Figure 27: Reference configuration (Configuration 3).

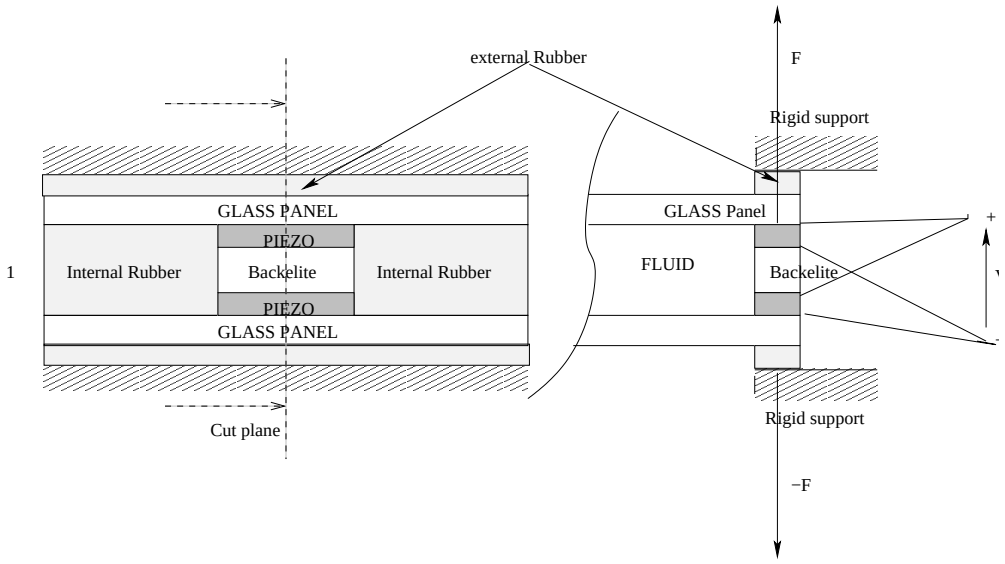


Figure 28: Actuators mounting in the experimental set-up.

in order to improve the controller efficiency. Different control loops are finally proposed.

## 3.6 Actuator optimization

Actuators employed here are made of piezoceramic material. Precisely of PZT kind. This material is nowadays of a great interest because as it can be used as an actuator or/and a sensor. Moreover, it can be easily shaped and integrated to mechanical structure. In Figure (28), an original mounting of piezoelectric actuators is drawn. It runs as a jack that generates opposite forces on each panel. The PZT patches used here are rectangular shaped materials with $4\,mm$ width. These forces are related to the applied voltage according to expression (26) that is derived and well presented in reference [18]. In fact, it can be readily established, that:

$$F = -\frac{d_{33} S_a}{s_{33} e_a}.V = -n_a.V \tag{26}$$

$F$ being the force delivered by the PZT for a given voltage $V$. $d_{33}$ designates the piezoelectric charge coefficient, $e_a$ being the piezoelectric actuator width, $S_a$ the piezoelectric element area and $s_{33}$ is the piezoelectric elastic constant. In the case of the piezoceramic used in this experiment, the constant $n_a$ is estimated to $n_a = 64NV^{-1}$. It should be noticed that such an actuator mounting is interesting for controller since it permits the generation of forces in the opposite way of those transmitted from one panel to the other through the cavity fluid and the rubber bands. The modal actuating equation of an

actuator $j$ located at $(x_j, y_j)$ was given in (19). In the control situation a term due to the piezoelectric actuator should be added. In fact, if the actuator $j$ is ordered a voltage $V_j$, equation (19) is transformed into the following expression (27):

$$\ddot{q_k} + 2\xi_k\omega_k\dot{q_k} + \omega_k^2 q_k = f_{inc}^k + n_a\phi_k(x_j, y_j)V_j \tag{27}$$

In our situation, as deeply discussed in the previous section, only two modes of vibration of the double glazing windows was retained. Henceforth, the presented application will use two actuators located respectively at $(x_1, y_1)$ and $(x_2, y_2)$ coordinate positions. Thus the actuating equation for the mode $k$ is given by:

$$\ddot{q_k} + 2\xi_k\omega_k\dot{q_k} + \omega_k^2 q_k = f_{inc}^k + n_a\phi_k(x_1, y_1)V_1 + n_a\phi_k(x_2, y_2)V_2 \tag{28}$$

Let us assume that both actuators are driven by the same command signal to act only on the out of phase moving panel modes. In addition, since the modes to control are symmetric, the actuators are assumed to be placed in symmetrical location. So that the identities $\phi_k(x_1, y_1) = \phi_k(x_2, y_2)$ and $V_1 = V_2$ are verified. Hence, equation (28) becomes simply:

$$\ddot{q_k} + 2\xi_k\omega_k\dot{q_k} + \omega_k^2 q_k = f_{inc}^k + 2n_a\phi_k(x_1, y_1)V_1 \tag{29}$$

Expression (29) is useful since it's necessary to look for the optimal locations of the actuators. These locations should guarantee the best performances and a minimal input energy necessary to the control. To achieve such an optimization, the controllability Grammian notion developed in references [19, 20, 21] is used. It depends only on the actuating term which is the term $2n_a\phi_k(x_1, y_1)$ (see equation 29) and measures the input energy of the actuators. Hac and Liu [19] shows that the optimization consists of maximizing the controllability Grammian in the direction of a given Euclidean norm. In case of light damping and well spaced natural frequencies, they show that the Grammian is dominated by its diagonal elements which are given, in our application, by expression (30) where the diagonal element $Q_k$ is associated to the $k_{th}$ mode:

$$Q_k = 4n_a^2\phi_k^2(x_1, y_1) \tag{30}$$

As both radiating modes $(1, 1)$ and $(3, 1)$ are considered in the control definition, the resulting index is:

$$Q = 4n_a^2(\phi_{11}^2(x_1, y_1) + \phi_{31}^2(x_1, y_1)) \tag{31}$$

Thus, the optimization consists of finding the coordinate location that maximize the terms associated to the radiating modes. The maximization of the considered quantity in equation (31) leads to the optimal locations described in Figure (29). In our situation, the shape of the piezoelectric actuator was

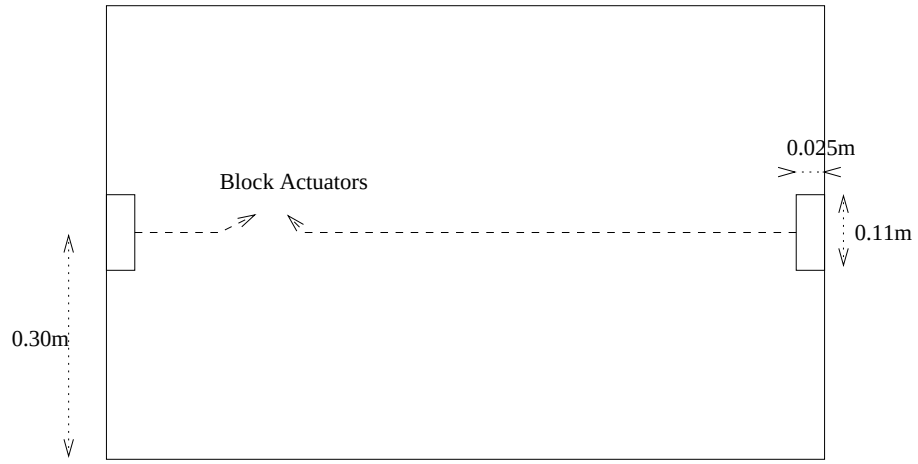


Figure 29: Optimal location of piezoelectric actuators

fixed. So the result of the optimization leaded only to the optimal location of patches. More details concerning such optimization technique can be found in [19, 20, 21], where some applications as well as deep discussions about the numerical implementation are given.

However, results of the Grammian optimization leading to the optimal locations represented in Figure (29) can be understood easily. In fact, as seen before, modes to be controlled are symmetric and out of phase motion of the panels. So, optimal locations found will correpond to a localy maximum remoteness of emitting and receiving panels.

### 3.6.1 The control loops

The objective of the proposed control is to minimize the modal energy of the two radiating modes identified in the previous sections. The optimal modal control strategy developed in [20] seems to be a suitable method. In this application, two sensors are needed to construct a modal filter that should extract the modal coordinates necessary to the command control. However, modal filtering and modal control may lead to heavy digital process making the control difficult to implement in real life conditions. Accordingly, for the double panel controller proposed here, is a simple feedback of either velocity of a particular point of the radiating panel or the pressure at the middle of the fluid cavity.

All the *associated control-loops* are summarized in Figure (30). Precisely, solid lines loop denotes two feedback controls using velocities signals picked up at points 1 and 2 as indicated in Figure (30). These points correspond slightly respectively to the antinodes of the radiating modes ($2nd$ and $3rd$ peaks shown in Figure (21)). The third solid line denotes the feedback controller using the

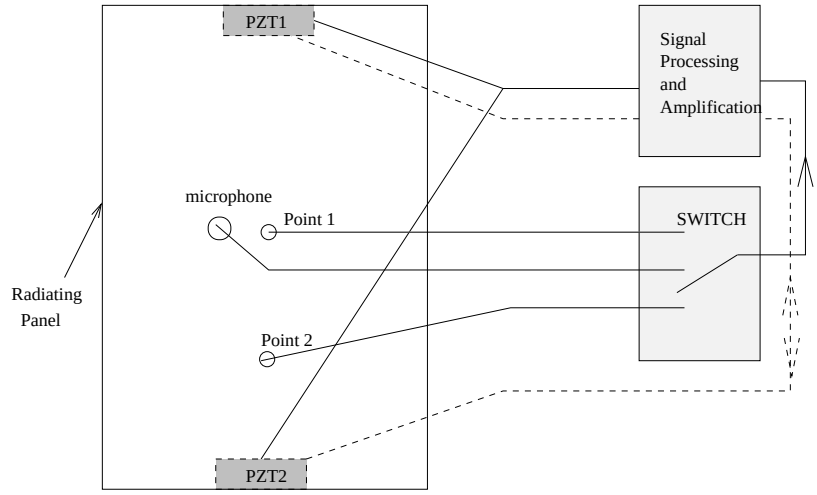


Figure 30: Control loops description

pressure signal measured in the center of the air cavity.

Finally, the dashed line denotes a feedback controller using the travel signal. The travel signal being the signal delivered by the piezoceramic patch. In fact, piezoceramic placed at the boundaries can be naturally used as sensors or as actuators. In this tentative , one block of piezoelectric actuators is used as a sensor to measure a signal which proportional to the travel signal and the second block is naturally used as an actuator.

So, to summarize, three controller was implemented in the double glazing window boundaries control: • the first one is designated in the following by velocities controller, • the pressure controller and finally, • the piezoelectric sensor based controller (travel control).

## 3.7 Experimental control results

This section summarizes experimental results showing the control performances. The attenuation level of the pressure of the fluid cavity is presented, in what follows.

To deal with a velocity feedback control, both accelerometers placed at points 1 and 2, are used in the tests. The measured signals are integrated to give the velocities. For the pressure and travel feedback controls, no particular signal processing on the pressure and travel signals is performed.

In all the closed-loop configurations the measured signal (velocities, pressure and travel) come through an amplifier and the amplified signal is applied to the piezoceramic actuators. A loudspeaker that is ordered a white noise in the frequency-range $0 - 400Hz$ serves as an acoustic perturbation source on the double panel partition.

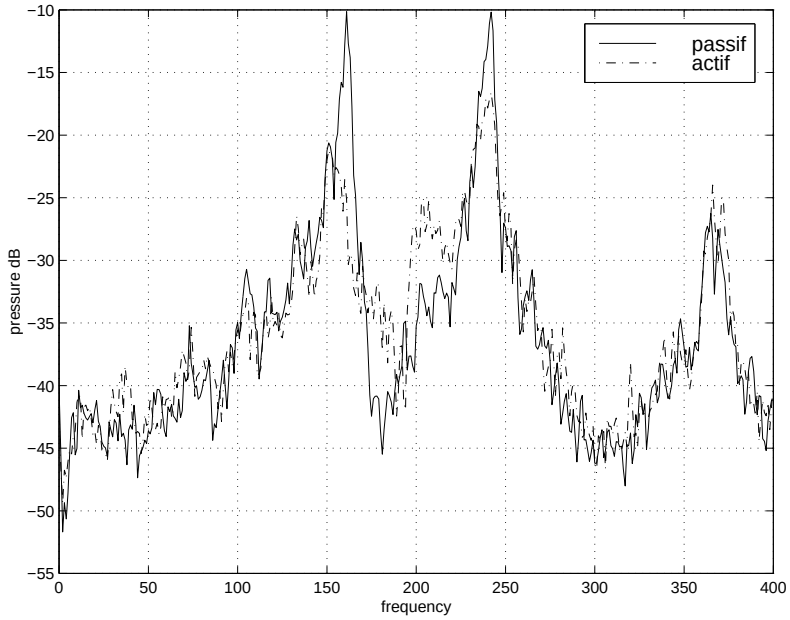


Figure 31: Pressure level at the center of the fluid cavity (*velocity feedback at point* 1*)*

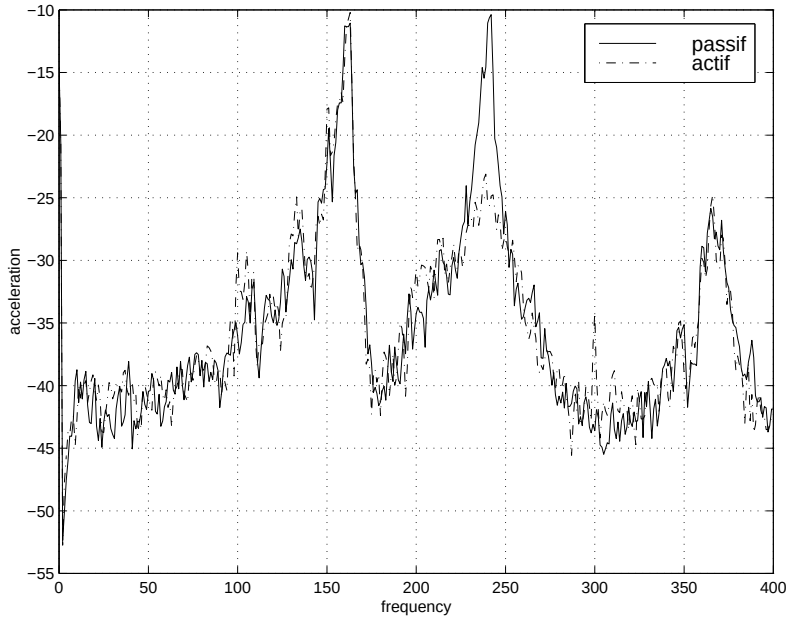


Figure 32: pressure level at the center of the fluid cavity (*velocity feedback at point* 2*)*

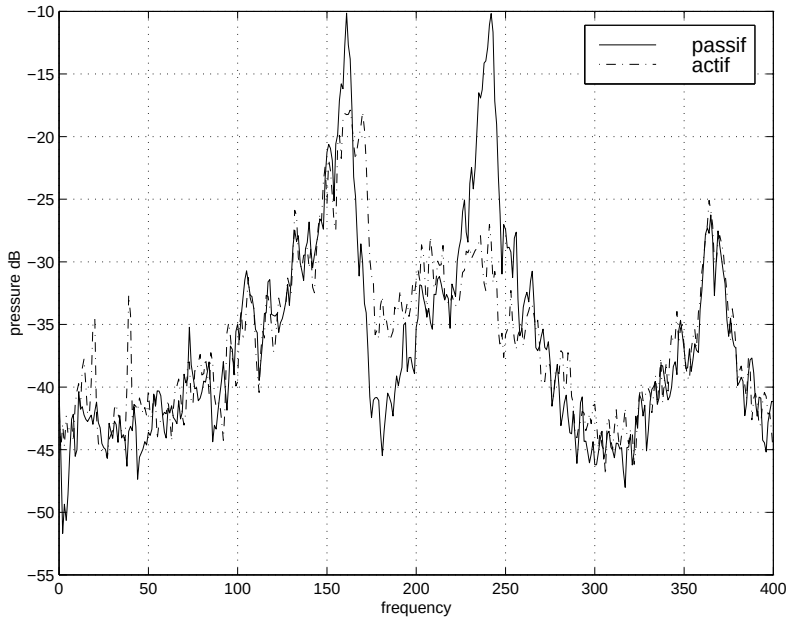


Figure 33: Pressure level at the center of the fluid cavity (*pressure feedback control)*

Figures (31) and (32) show that the control performance is better on the first resonance if the feedback of velocity at point 1 is used and better on the second resonance if the feedback of velocity at point 2 is used. This is because the modal participation of the first mode for example is more important at point 1 and less at point 2. In other words, this mode is more observable at point 1 than at point 2.

On Figure (33), is plotted the curve performances of the pressure feedback control. These performances are comparable to those obtained by the velocity feedback control. However, the last control is efficient on both resonance peaks because the associated radiating modes participate in equivalent way on the pressure level.

Finally, Figure (34) shows the control result of a travel feedback. The performances are limited to almost $9\,dB$ around the second peak. It should be possible to improve better performances if the two existent blocks as actuators and a new block as a sensor are used. All the result of control are summarized in Table (6):

Table 6 shows clearly that an improvement has been achieved with a simple analog controller proving the feasibility of the boundary controller.

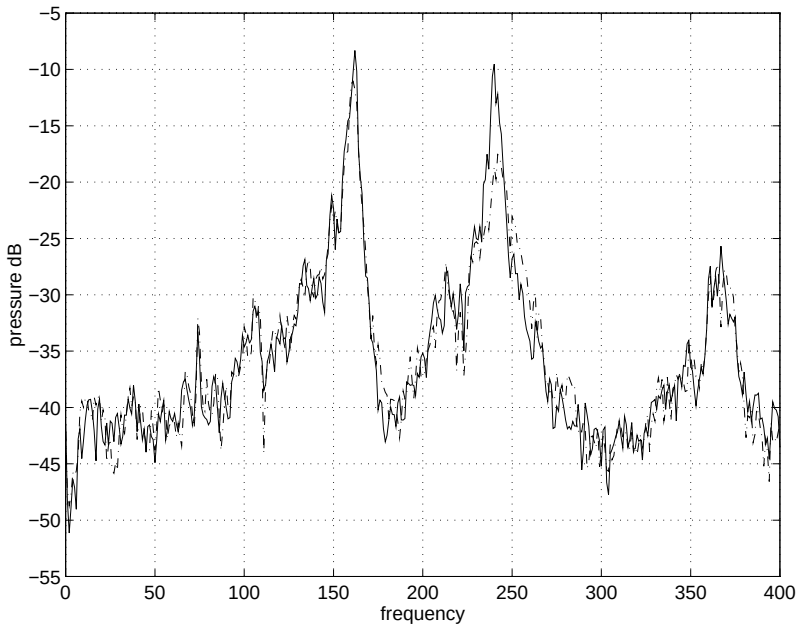


Figure 34: Pressure level at the center of the fluid cavity (*travel feedback control)*

| feed-back Signal | Velocity $P_1$ | Velocity $P_2$ | Air gap pressure | Travel |
|---|---|---|---|---|
| Gain control on $1^{st}$ pick (dB) | 10 | 0 | 7 | 3 |
| Gain control on $2^{nd}$ pick (dB) | 8 | 15 | 18 | 9 |

Table 6: Double panel partition gain control

### 3.8 Concluding remarks

This section has investigated an original scheme of active control of double panel partition using piezoelectric elements. The studied configuration is an alternative control strategy to classical acoustical or structural control. In fact, the generated structural forces are located on the boundaries.

Hence, using a modal expansion technique, it turns out that the symmetric and out phase modes are the most radiating ones. In particular, the study of the mass-air-mass mode shows its dependency on the rubbers and panels stiffness as well as the air gap characteristics. For the realistic case, much more radiating modes appear and the mass-air-mass mode is not yet a valid notion. To dump out these modes, a structural control is investigated to minimize their modal energy. Two piezoelectric actuators are optimized using the Grammian controllability notion.

The performed tests using a proportional controller to velocity or air gap pressure shows the efficiency of such a structural control. The optimization of the actuators leads to a high attenuation of the radiated power level. In a last test, the use of the piezoelectric components as sensor and actuator was shown to be possible even the attenuation level is not very important. That's why it should be interesting to think about an actuator that permits the generation of more energy on the system.

## 4 General conclusions

Active/passive systems as a mean for reducing vibration levels is a very key point in most industries, as in car, automotive, aeronautic and space industries. In this chapter, the combination of piezoelectric materials and smart structures for that purpose has been investigated. At first, a new concept of rubber mount has been analysed. An adjonction of a piezoelectric block to the rubber mount, to increase its efficiency, has been studied. 10 dB attenuation can be obtained for a white noise excitation within the frame of an increased limited cost with regards to control algorithm and devices. This concept could be very useful for controlling acceleration levels at mounting points of equipment installed on spacecrafts, for example. Then, an innovative mean of active control of double panels has been investigated. The analysis has pointed out the significant role of structural radiating modes compared to mass-air-mass modes. Consequently, a structural control using two piezoelectric actuators, with a proportionnal controller to velocity or air gap is very efficient, and leads to high attenuation of the radiated power level. Hybrid passive/active control systems have great potentialities for reducing acoustic vibration levels, for example, for attenuating acoustic environment in aircraft cockpits or at payload/launch vehicle interface.

# References

[1] Wiener. *Extrapolation, Interpolation and Smoothing of Stationary Time Series, with Engineering Applications*. Wiley, New York, 1949.

[2] Widrow and Stearns. *Adaptive Signal Processing*. Prentice Hall, New Jersey, 1985.

[3] Orfandis. *Optimum Signal Processing*. MacMillan, New York, 1985.

[4] Michaut. *Méthodes Adaptatives pour le Signal*. Hermes, Paris, 1992.

[5] Ljung. Analysis of recursive stochastic algorithms. *IEEE Trans. AC-22*, 24, 1977.

[6] R. Paurobally, J. Pan, and C.Bao. Feedback control of noise transmission through a double panel partition. In Ft Lauderdale USA, editor, *Active 99 congress*, number Vol 1, pages 375–387, 1999.

[7] A. Jacob and M. Moser. Enhancement of the transmission loss of double panels by means of actively controlling the cavity sound field. In Ft Lauderdale USA, editor, *Active 99 congress*, number Vol 1, pages 1–12, 1999.

[8] S. Pietrzko and O. Kaiser. experiments on active control of air borne sound transmission through double wall cavity. In Ft Lauderdale USA, editor, *Active 99 congress*, number Vol 1, pages 355–363, 1999.

[9] C. Lesueur. *Rayonnement acoustique des structures*. Editions Eyrolles, Paris, 1988.

[10] B. Pascal, J. Rolland, and L. Gagliardini. Dispositif d'atténuation acoustique à double paroi active. Centre Scientifique et Technique du Batiment, 95. Brevet d'invention $N^o$ 2704969.

[11] P. Sas, F. Augusztinovicz C. Bao, and W. Desmet. Active control of sound transmission through a double panel partition. *journal of sound and vibration*, 4(180):609–625, 1995.

[12] A. Sampath and B. Balachandran. Studies on performance functions for interior noise control. *Smart Materials and Structures*, 6:315–322, 1997.

[13] A. Sampath and B. Balachandran. Active control of multiple tones in an enclosure. *Journal of the Acoustical society of America*, 106(1):211–225, 1999.

[14] C. Bao and J. Pan. Experimental study of different approaches for active control of sound transmission through double walls. *journal of Acoustical Society of America*, 102:1664–1670, 1997.

[15] J. P. carneal and C. R. Fuller. Active structural acoustic control of noise transmission through double panel systems. *journal of AIAA*, 33(4):618–623, 1995.

[16] P. Gardonio and S. J. Elliot. Active control of structure-borne and airborne sound transmission through double panel. *AIAA paper*, 23(53):864–879, 1998.

[17] L. Meirovich. *Dynamic and control of structures.* John Wiley and Sons Publication, 1989.

[18] D. Bondoux. Piezo_damping of light structures : modelling and experimental results. In C. L. Kirk and D. J. Inman, editors, *Space96/3rd international conference on dynamics and control of structures in space - Cranfield university - Londres*, number 143, pages 229–248, 1996.

[19] A. Hac and L. Liu. Sensors and actuators location in motion control of flexible structures. *Journal of Sound and vibration*, 2(167):239–261, 1993.

[20] B. Jemai, M.N. Ichchou, and L. Jezequel. An assembled plate active control damping set-up: Optimization and control. *Journal of Sound and vibration*, 225(2):327–343, 1999.

[21] M. Collet and L. Jezequel. Active modal control with piezoelectric layers optimisation. *Journal of Structural Control*, 1(2), 1994.

**Received: April 27, 2007**